

4. Modern Submillimetre Microwave Scanning Spectrometry

A. F. KRUPNOV

Applied Physics Institute, U.S.S.R. Academy of Sciences, Gorky, U.S.S.R.

1. Introduction	217
2. Novel Developments in the Theory of Spectrometry with a Coherent Radiation Source	221
2.1. A New Method for Obtaining Sub-Doppler Resolution in Gas Spectrometers	222
2.2. New Possibilities for Spectroscopic Measurements under Conditions of Spectral Line Saturation	225
3. Modern Construction of RAD Spectrometers	226
3.1. Scanning Sources of Submillimetre Coherent Radiation	226
3.1.1. Fast Broad-band Scanning of the BWO Output Frequency . .	227
3.1.2. Precise Digital Scanning of the BWO Output Frequency. .	231
3.2. The Cell and the Detector	235
3.2.1. Calculation of Optimal RAD Cell and Detector Parameters .	235
3.2.2. Construction and Operation of the Cell and Detector of a RAD Spectrometer	238
4. Practical Methods of Investigation in Submillimetre Microwave Scanning Spectrometry	241
5. Conclusion	248
References	248
Appendix 1. Calculation of Sub-Doppler Spectral Line-shapes	251
Appendix 2. Calculation of the Line-shape and Magnitude of the Signal from Lines in RSC Spectrometry under the Condition of Line Saturation	254

1. INTRODUCTION

For a very long period of time, the sensitivity of the techniques available to the submillimetre spectroscopist were so significantly behind those available in the neighbouring microwave and infrared regions that the constant reference to the "submillimetre spectroscopic gap" was fully justified. Initially the submillimetre region was explored by extending the capabilities of the familiar infrared spectrometers to longer wavelengths. These spectrometers are equipped with a thermal (i.e. hot black-body) source and they therefore have the advantage that a wide spectral range can be readily scanned. One can get therefore a broad continuous picture of the region to be investigated and this can give a wealth of information and be of

considerable heuristic significance. The disadvantages all stem from the low power per unit frequency interval of black body sources. This means that the resolving power will always be low and the sensitivity poor.

The first penetration into the submillimetre range from the microwave side was made in the forties and fifties using microwave spectrometers having a classical layout appropriate for the centimetre-band scheme of operation but using a harmonic generator as the source of the coherent radiation [1]. This first microwave approach to the submillimetre range made possible substantial increases in the resolving power, the accuracy of measurement of the line frequency and (with the further development of the technique) the sensitivity of these spectroscopic methods when compared with the infrared-type incoherent ones. However, in comparison with the microwave spectrometers in the centimetre region which had quickly achieved sensitivity and resolving power values close to the theoretically predicted limits for this type of spectrometer [2], these submillimetre microwave spectrometers, of the first generation, had some orders of magnitude poorer sensitivity and they were not able to scan a broad range of frequencies. These disadvantages were mainly due to the low efficiency of harmonic multiplication which meant that there was little power in the harmonics and also to the complexity of the radiation spectrum produced by the harmonic generators. However, there were other difficulties such as the problem of broad-band tuning, the increasing problem of mode interference in the oversized guides, the worsening of receiver characteristic with increasing frequency as well as the inefficiency of the conventional methods of signal recovery. Nevertheless the great skill of the experimenters working in this field made it possible to obtain submillimetre spectroscopic data on a large number of molecules; but the inefficiency and complexity of these methods prevent their being suitable for the extensive spectroscopic exploration of the submillimetre region of the spectrum (for example the development of commercial spectrometers, spectral catalogues, etc.). A systematic presentation of the state-of-the-art of these techniques has been given in some recent books [3, 4, 5].

The appearance of broad-band primary sources of coherent submillimetre radiation with considerably larger power—the backward-wave oscillators (BWOs) [6]—has stimulated new efforts in the development of scanning submillimetre spectrometers. In this connection, the pioneering work of A. M. Prokhorov and his co-workers should be especially mentioned [14]. However, to make the most effective use of such radiation sources in a microwave gas spectrometer, it was necessary to develop adequate broad-band and frequency-independent receivers, to devise effective means of recovering useful spectral line signal and to have available methods of control and measurement of the output frequency of these

coherent sources over a broad continuous range. To satisfy these requirements it first proved very useful to adopt the concept of spectrometer design in which changes in some parameter of the specimen (its temperature for example) are monitored rather than to follow the older practice in which one detects changes in the radiation after it has traversed the specimen [7]. To realize this concept for the particular case of a microwave spectrometer it is convenient to use the well known and proven method of acoustic detection† [8].

The scanning spectrometer developed on the basis of broad-band submillimetre backward-wave oscillators and acoustic detection was called RAD [7, 9] (from the initial letters of the phrase “radio-spectroscope with acoustic detection”). The development of this spectrometer led to an increase of the available signal-to-noise ratio from values of typically 1–10 up to some millions. With the addition in very recent years of the system of precise digital control of the submillimetre BWO output frequency it has been possible to increase the accuracy of frequency measurements in this region to one part in 10^8 or even one part in 10^9 , and the range of scanning microwave spectroscopy has been extended more than an order of magnitude up to frequencies greater than 1 THz. These advances have been secured with an experimental system so simple that it is readily adaptable for commercial exploitation.

The availability of scanning microwave spectrometers in the submillimetre region opened a new field of spectroscopy, since prior to this development the sensitivity, resolution limits and accuracy of frequency measurement of the alternative methods were all much lower (see the next chapter). The new spectrometers, moreover, compared very favourably with coherent spectrometers in either of the adjoining microwave or infrared regions. Thus they had broader spectral coverage than the centimetre scanning microwave spectrometers and they could readily better the frequency precision of coherent scanning infrared spectrometers (for example the spin-flip Raman laser). These advantages were secured without loss of sensitivity. Figure 1 shows the spectral regions covered by the three coherent scanning systems. The “information yielding power” of a spectroscopic method will be defined by its sensitivity, its precision of frequency measurement and its bandwidth and there is thus every reason to suppose that the main interest in microwave spectroscopy will continue to

† This method is particularly suitable but one can readily think of others. Thus for solid and liquid samples one might use the circuit given later for determining small ($\Delta C/C \sim 10^{-11}$) variations of capacity for registering the corresponding variations of the dielectric constant of the sample ($\Delta\epsilon/\epsilon \sim 10^{-11}$) under the action of radiation. For gaseous specimens, an attractive proposition is to use the coherent spontaneous radiation from molecules previously excited by the radiation from the source.

be (see Chapter 1) at its high-frequency limit and this at present lies in the submillimetre range.

The spectroscopic potential of the submillimetre region is enhanced by the lucky coincidence that the maxima of intensity of the rotational spectra of a large number of molecules of interest lie in this range. Submillimetre spectroscopy has its own "distinguished class of spectra". This is illustrated in Fig. 1 where is shown the envelope of the room-temperature rotational spectrum of OCS. The potential of the high sensitivity of the method

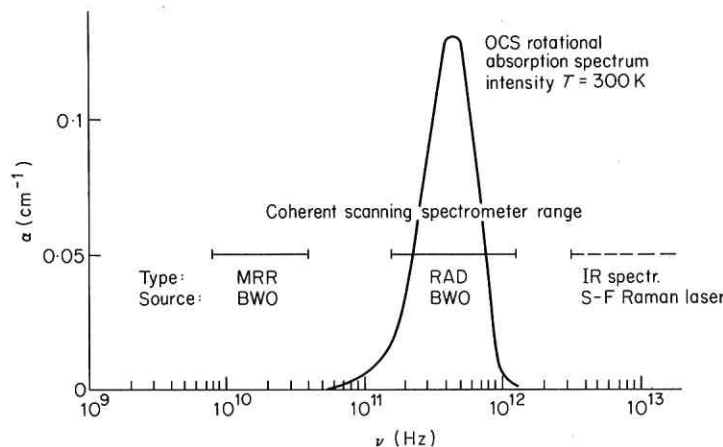


FIG. 1. The region covered by coherent submillimetre scanning RAD spectrometers and the region of maximum intensity of OCS rotational lines (at 300 K). For comparison are shown the neighbouring regions which are covered by coherent scanning spectrometers; microwave MRR [24] and infrared with spin-flip Raman lasers [31]. The existing upper end of precise microwave methods of scanning the frequency lies at approximately 1100 GHz. For lower frequencies the typical accuracy of scanning of the frequency reaches $\sim 10^{-8}$ - 10^{-9} but for higher frequencies only $\sim 10^{-5}$ [23, 24, 27, 31].

coupled with the maximum of intensity, for detecting the rotational spectra of molecules present at low concentration (free radicals for example) is obvious. The present stage of development of submillimetre scanning spectrometry provides a solution to the practical needs of those exploring the submillimetre region at very high resolution. Earlier steps in the ongoing programme of development are described in a review [9]. This chapter describes further developments of new methods of submillimetre microwave scanning spectrometry and also analyses some related consequences of these methods.

2. NOVEL DEVELOPMENTS IN THE THEORY OF SPECTROMETRY WITH A COHERENT RADIATION SOURCE

It was mentioned above that for the development of scanning submillimetre spectroscopy it is rather useful to employ spectrometers in which the signal from spectral lines is registered as a change, in a sample parameter investigated, under the action of radiation (RSCS, see Table 1) [7, 9]. In practice, based on this conception, a submillimetre scanning spectrometer, RAD, has been developed; but the RSCS conception proved to be significantly broader and leads, in particular, to a re-estimation of the sensitivity limits of microwave spectrometers and to some new suggestions for techniques and methods of spectrometry. These will be given in the present chapter. The main consequences of RSCS application, mentioned earlier, are the possibility of considerable sensitivity increase in comparison with RRCS (Table 1), the independence of the sensitivity on the frequency and the absence of false signals [7, 9].

The RSCS sensitivity independence of the frequency makes possible the elimination of the large difference in sensitivity between the submillimetre and the centimetre ranges and is rather valuable for the realization of the scanning spectrometer regime which can be achieved in RSCS merely by scanning the radiation source frequency.

The elimination in RSCS of the majority of the false signal sources is also valuable for the realization of the scanning regime since it gives the possibility of recording large parts of the spectrum at the maximum sensitivity.

TABLE 1. General classification of spectrometers according to the method of signal formation from spectral lines

I	Registering Radiation Changes Spectrometers	RRCS with radiation receivers
IIA	Registering Sample Changes Spectrometers	RSCS with microscopic parameters receivers ("particles-in-the-level-counter" type)
IIB		RSCS with macroscopic parameter receivers ("acoustic detector" type)

Especially noted should be the possibility of increasing microwave spectrometer sensitivity associated with the use of RSCS. In references [7] and [9] there are given some estimations; they show that even spectrometers of the RAD type (registering the change of macroscopic gas parameters) may have better sensitivity in comparison with the conventional microwave Stark spectrometers. But the use of RSCS with a receiver of the type of "particles-in-the-level counter" will give essentially higher spectrometer sensitivity. Still more promising may be devices with receivers depending on the coherent parameters of molecular ensembles, the theory of which is now being developed. The creation of such spectrometers would be in our opinion the next important step in the development of microwave spectrometry.

New theoretical consequences of the use of RSCS, considered here, are rather general principles of the spectral line-shape and width control [10] and the possibility of obtaining additional information under conditions of spectral line saturation.

2.1. A New Method for Obtaining Sub-Doppler Resolution in Gas Spectrometers

At present there are two main directions for eliminating the Doppler line-broadening in gas spectrometers. Firstly one may select a group of molecules with a narrow spread of velocities about a mean (usually zero) or secondly one may use a means for compensating (i.e. subtracting) the Doppler shift. The selection method, of which the archetype is molecular beam spectroscopy, requires the physical separation of the molecules with the desired velocities from all the others. The group when separated will have a highly non-thermal velocity distribution. This is an illustration of the general principle that to obtain sub-Doppler resolution it is necessary to disturb the thermodynamic equilibrium of the gas.

It is worth noting that the interaction of an intense coherent wave with a gaseous sample is a non-equilibrium interaction and one may invoke this non-equilibrium to obtain sub-Doppler line-widths. In quantum terms the primary effect of the resonance radiation action on the gas is to change the population of the resonant levels of the set of molecules whose velocities correspond to the radiation frequency. In other words one "burns a hole" in the population distribution. To then separate a group of molecules with zero Doppler frequency shift it is necessary to set up for the molecules a system of coordinates *fixed relative to the radiation source*. This may be done in only two ways: firstly by the radiation field itself (by for example setting up a standing wave pattern when the radiation passes through the cell twice in opposite directions), or secondly by mechanical means, using

the cell walls, diaphragms, etc. The first way corresponds to the Lamb dip non-linear method [11, also Chapter 3]. The second way corresponds to a new linear method of obtaining a sub-Doppler line-width, but one that may only be realized in RSCS spectrometry.

The realization of this new form of sub-Doppler spectroscopy in RSCS is based on the two-stage nature of the formation of the signal in this class of spectrometer. In the first stage a particle (for example a molecule in the gas phase) interacts with the radiation field and absorbs a quantum of radiation. At the second stage this excited particle is registered either directly by a counter of excited particles† or else indirectly through the effect it has on the macroscopic parameters of the gas. In either way a signal is created corresponding to the absorption line. Now clearly we may physically separate the regions of absorption and detection and if a set of diaphragms and baffles is set up inside the cell, we can ensure that the molecules delivering the excitation to the detector will have an almost zero velocity component in the direction of the beam. Excited molecules having large Doppler shifts, i.e. moving with significant components along the direction of the normal to the wave front will not reach the detector but will instead lose their excitation in collisions with the walls or with the diaphragms. The RSCS receiver will therefore only register signals corresponding to the central part of the Doppler line and there will be a considerable line-narrowing. The process is strongly akin to molecular beam methods and here the geometrical angle defined by the diaphragms plays the same role as does the angle of divergence of the molecular beam in beam methods, but this method is free from some of the drawbacks of beam methods, such as the necessity to have permanent pumping, etc. The operation of line-width reduction in RSCR, by velocity selection as compared with the non-selective full Doppler-broadened operation of an RRCS spectrometer is illustrated in Fig. 2. Of course for effective line-narrowing it is necessary to fulfill some conditions on the mean free path of the molecules l_f , the dimensions of the plane wave front R , the geometrical angle (radians) of the diaphragm aperture θ and the wavelength of the radiation λ . In fact one must have

$$l_f \gtrsim R \gg \lambda; \quad \theta \ll 1. \quad (2.1)$$

The calculation of the shape of sub-Doppler lines obtained by this technique is detailed in Appendix 1 and is shown in Fig. 3.

†The receiver of excited particles may be for example a detector which relies on surface ionization by metastable atoms, or a photomultiplier which detects the fluorescence from the excited atoms or molecules or a thermal acoustic receiver. In the last case the receiver is a sufficiently large (to ensure thermalization of the gas) chamber fitted with a microphone. Finally the coherently excited ensemble of particles may be detected by the reception of their coherent spontaneous emission of radiation.

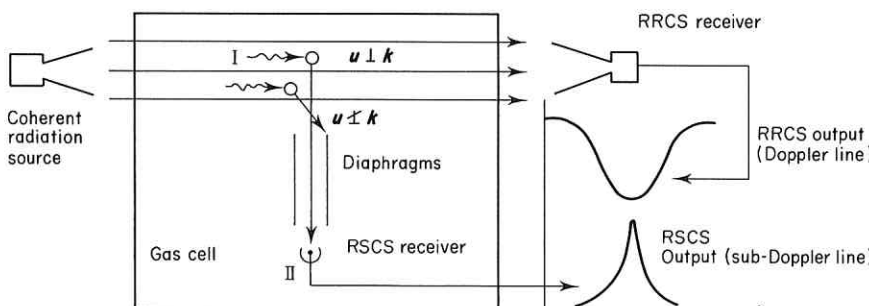


FIG. 2. A new method of obtaining sub-Doppler lines in gas spectrometers of RSCS type. Molecules are excited by the radiation from the coherent radiation source; diaphragms (partitions), before the receiver of excited molecules, select only Doppler-free molecules, the velocities of which are perpendicular to the direction of the radiation propagation ($u \perp k$). Molecules for which $u \pm k$ strike the diaphragm. On the right are shown the forms of the output signals for the spectral lines obtained in the same gas cell with frequency scanning: sub-Doppler from RSCS detector (excited molecule detector) with molecule velocity selection and full Doppler from RRCS detector.

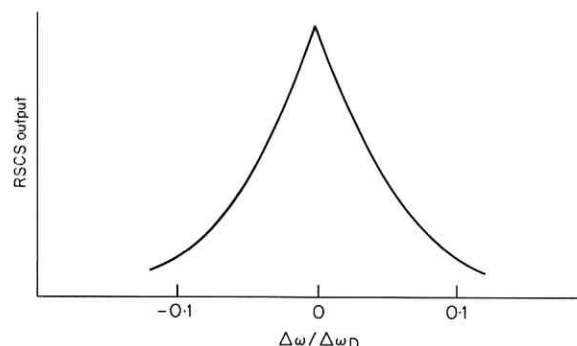


FIG. 3. Calculated shape of the sub-Doppler line for the RSCS cell of Fig. 12 (Appendix). $\theta = 0.1$ and vanishingly small homogeneous line-width. In real conditions the peak is "rounded" by homogeneous (for example, time-of-flight) broadening. The scale along the frequency axis is in units of the Doppler line HWHM.

This new method completes, in principle, a certain class of methods for sub-Doppler operation based on velocity selection. What remains to be done is to determine the possible range of application of the method. This will depend on its inherent peculiarities namely that it is linear, it involves only a single passage of the beam through the cell and the line is properly recorded from a true zero level (not in the form of a dip as in the non-linear methods). It is possible that the optimum spectral region for the application of this method may be at shorter wavelengths, since there each molecule arriving at the detector will be bringing more energy and of course the

starting Doppler width is that much greater. Additionally, the intensity of spontaneous radiation also increases with increasing frequency. As an example it may be shown that the sensitivity of the new method in the particular case of observation of the excited particles by their fluorescence exceeds the sensitivity of the non-linear fluorescence method considered in [12] especially in the case of small intensity of the radiation field. This method may also be used to realize a "space-resolved" microwave spectrometer depending on the coherent spontaneous emission of radiation by the molecules.

2.2. New Possibilities for Spectroscopic Measurements under Conditions of Spectral Line Saturation

The regime of spectral line saturation is used for various purposes in microwave spectroscopy. Thus we have already seen in Chapter 1 how it may be used to provide a means of modulating a microwave spectrometer. It may also be used as an aid to quantitative measurement. Thus Harrington [13] has illustrated this for Stark spectrometers (i.e. the RRCS type) where the saturation effect is used for a specific calibration which permits the determination in quantitative terms of the concentrations of the various species present in the mixture and that is of course the whole practical analytical problem. Since the variation of signal with incident radiation power is different in RRCS and RSCS the use of the latter opens some new possibilities for spectroscopic measurements under the saturation regime. RSCS also offers the advantage that, since it is possible to use considerably larger radiation powers than are convenient in RRCS, it is possible (in principle, anyway) to achieve the saturation regime over a broader range of the experimental conditions.

In contrast to Stark-modulated spectrometers where, as the radiation power increases, the signal from the lines first passes through a maximum and then tends to zero [13], in RSCS the amplitude of the signal at the centre of the line only is saturated. The details of the calculation of the shape and of the amplitude of the spectral line signal observed are given in Appendix 2. At large values of the saturation parameter, the signal amplitude (for RSCS) at the centre of the line is proportional to the population of the lower level and does not depend on the power passing through the cell. The line-width, on the other hand, under these conditions is proportional to the matrix element of the transition and to the square root of the radiation power. It therefore follows that in RSCS it is possible to determine the lower level population and the transition matrix element separately unlike the case for RRCS where these two quantities always occur as a product [2, 13]. Following on from this, the possibility arises of

using RSCS measurements under the saturation regime as an aid to making assignments especially for broad-band sweeps. One looks for lines with the same signal amplitude and assumes these to have also the same or close-lying lower levels. It should be noted here that the line-shapes expected are close to the Lorentzian form (see Appendix 2). A final point is that it is possible to achieve an absolute calibration of the sensitivity (i.e. to determine line-intensities absolutely) in RSCS spectrometers by registration of the maximal signal value from the lines together with some additional measurements. These would include a measurement of the gas pressure in the cell and just a few frequency measurements to define the statistical sum, i.e. the structure of the molecular levels and the widths and the frequencies of the spectral lines.

3. MODERN CONSTRUCTION OF RAD SPECTROMETERS

A submillimetre RAD spectrometer consists of a scanned source of coherent submillimetre radiation (a BWO) with devices for radiation frequency control and frequency measurement together with an absorption cell (or cells) fitted with a microphone. The microphone is followed by the usual microphone circuits, amplifiers, synchronous detectors, etc., and the chain ends in a two-channel recorder. The devices considered in this section are those which correspond to the two principal modes of operation of the RAD spectrometer namely broad-band survey sweeps with a non-stabilized BWO and precise relatively narrow-band scans with the BWO stabilized against an accurately known reference signal.

3.1. Scanning Sources of Submillimetre Coherent Radiation

The development of submillimetre scanning microwave spectrometers became a practical possibility only when backward wave oscillators covering this region became available. These sources have a monochromatic output, a "one-handle" frequency control and broad-band tuning capabilities. The main characteristics of the submillimetre BWOs which have been developed in the U.S.S.R. are shown in Table 2 [6]. Methods of frequency control and frequency measurement to be used with them are described below.

3.1.1. Fast Broad-band Scanning of the BWO Output Frequency

Scanning of the BWO output frequency without stabilization is used to obtain the general picture of the spectrum over a broad frequency range. A frequency scale is set up on the record by simultaneously recording a

4. MODERN SUB MM MW SCANNING SPECTROMETRY

known reference spectrum. A block diagram of the RAD device intended for this regime of work is given in Fig. 4. When the BWO is supplied from a sufficiently stable driving unit and it is operating in a single-frequency mode of oscillation† its oscillation is quite monochromatic: even in the non-stabilized regime the BWO radiation spectrum was sufficiently pure that sub-Doppler lines as narrow as 20 kHz [15] could be observed in a fast sweep. However, in this regime the long-time stability of the BWO frequency is rather unsatisfactory (hundreds of MHz) due to the strong dependence of the oscillation frequency on a number of parameters, the

TABLE 2. Main characteristics of submillimetre BWOs [6]

Operating frequency range (GHz)	Magnetic field strength (kOe)	Magnetic pole-to-pole distance (mm)	Maximum applied voltage (kV)
175– 270	6	22	4
250– 375	7	22, 30	4
370– 535	9	30	4
530– 715			
710– 940			
925–1250			
1200–1500	10–12	40	6–6.5

Notes: (a) BWO current no more than 50 mA. (b) Output power varies from tens of milliwatts in the low-frequency region to 100 microwatts near 1500 GHz [6].

most important of which is the high voltage supply. In recording a broad-band spectrum with RAD and an unstabilized BWO, the mode of operation has to be a compromise between going slow enough to match the slow response of the thermal detector and going fast enough that BWO frequency drift does not seriously distort line profiles. The "local" frequency scale on the chart record will then be, of course, not constant but this can be easily taken into account by consideration of the reference spectrum. In practice there is little problem and the range of allowed scan rates is large enough to record most spectra. Difficulties only arise when one is trying to achieve resolution better than 10^{-4} or 5×10^{-5} at a time constant of 1 s.

† The BWO may sometimes oscillate on two neighbouring modes of the slow-wave structure (either simultaneously or else jumping from one to the other). This phenomenon is, from a spectroscopic point of view, similar to that of "ghosts" which appear in the operation of diffraction grating spectrometers. The control of the BWO into a one-frequency regime is made using a known spectrum record: the principal experimental point is to ensure that the BWO is properly adjusted relative to the focusing magnetic field.

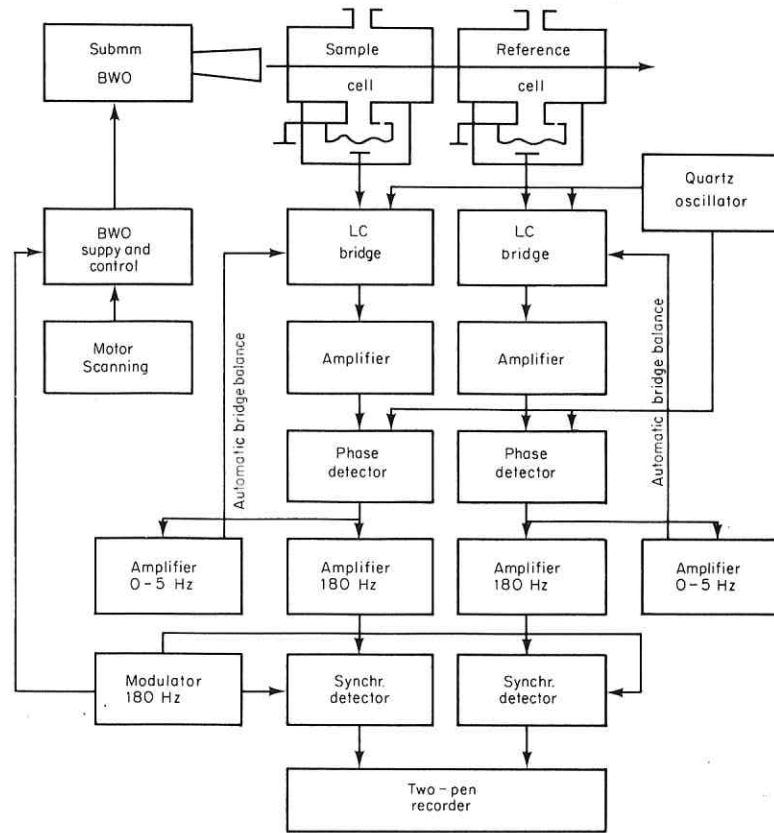


FIG. 4. RAD spectrometer for fast broad-band scanning of the spectrum with moderate resolution in the range 150–1100 GHz and frequency reading from a reference spectrum. As the frequency is scanned the spectrum investigated (sample in one cell) and the reference spectrum (sample in another cell) are recorded simultaneously. The region of scanning in one experiment amounts to some hundreds of gigahertz (see Table 2).

A block diagram of a suitable supply unit [16, 17] for a scanning BWO in a broad-band RAD spectrometer is given in Fig. 5. It is basically a servo-system which reproduces an input reference voltage at a much higher power level and scaled by the feedback parameter β^{-1} . The reference voltage is scanned by a motor and the output voltage follows it. The source of the reference voltage and the potentiometer for providing the linear scanning must provide relative stability and a scanning step value of nearly 10^{-5} . This is achieved by the use as the source of the reference voltage of a multistage parametric stabilizer featuring silicon stabiilitrons with stability

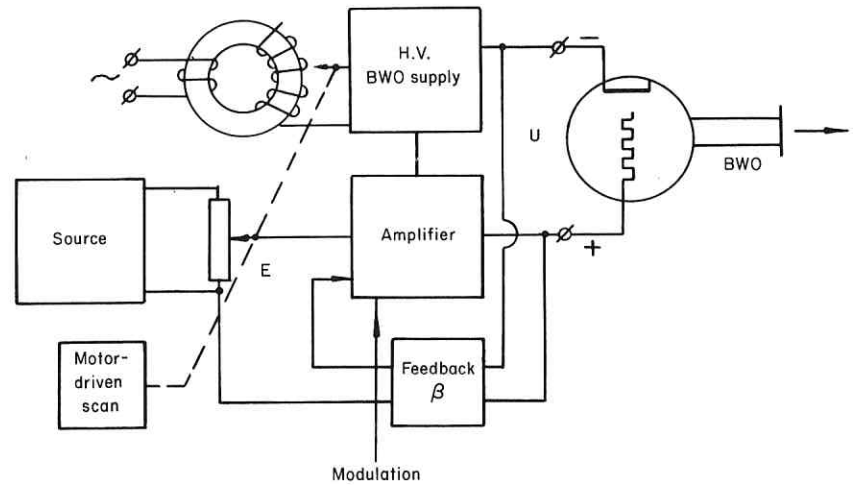


FIG. 5. Block-diagram of scanning stable supply source for the BWO used for the recording of survey spectra with the RAD spectrometer.

characteristics of $10^{-5}/^{\circ}\text{C}$ and as the divider a precise multiturn potentiometer driven by a synchronous motor with variable gearing.

Deviation of the output voltage U from the desired value $\beta^{-1}E$ may be due to an insufficient amplification coefficient K_e or else to drift of the D.C. amplifier. To provide the required quality of stabilization, the value βK_e of the stable source in this system amounts to 5×10^6 and the drift is reduced to $\sim 0.1 \text{ mV}/^{\circ}\text{C}$ by employing an amplifier built on the "modulator-amplifier-demodulator" principle in which the main amplification takes place at a high carrier frequency. The amplitude/frequency characteristic of the amplifier must satisfy the twin requirements of reproducing the square-wave modulation envelope without serious distortion and also of providing stable amplification. The modulation waveform has an amplitude up to 50 V with a frequency of 180 Hz and the stability requirement is that the amplitude/frequency characteristic should have a slope of less than 20 dB/decade except for the region where $|\beta K_e| < 1$. The design compromise chosen is to have an amplifier bandwidth of nearly 0.5 MHz and to choose an amplitude/frequency characteristic of the form

$$|\beta K_e| = (5 \times 10^5)/\nu \quad (3.1.1)$$

for frequencies greater than 0.1 Hz. This is achieved by the use of correcting filters.

The system described provides a power supply and a modulation for the BWO in the range 500–5000 V (currents up to 50 mA) with residual pulsations no more than 2 mV, drift no more than 50 mV (at the maximum

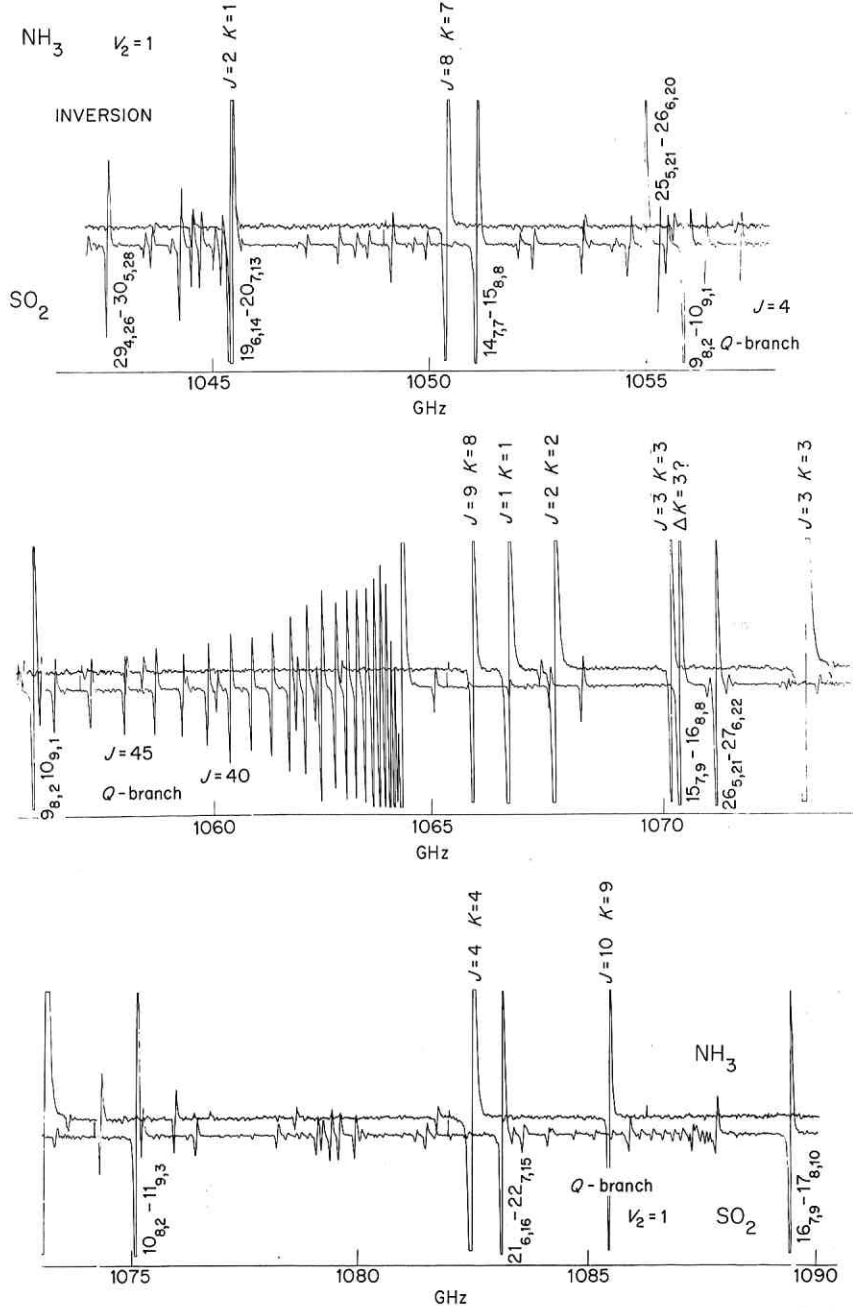


FIG. 6. Record of a part of the inversion spectrum of NH_3 in the excited vibrational state $v_2 = 1$ and the reference SO_2 spectrum in the frequency region near a 1 THz obtained with a RAD spectrometer; frequency marks in GHz.

voltage) and BWO scanning rates from 150 MHz/sec^{-1} down to 5 MHz/sec^{-1} . At the present stage of development, the scanning range of the non-stabilized BWOs is nearly 1 THz. This is illustrated in Fig. 6 which shows an ammonia spectrum† in the 1 THz region plus a reference SO_2 spectrum. The ammonia lines arise from inversion splitting in the $v_2 = 1$ vibrationally excited state. The ammonia inversion spectrum in the ground vibrational state (at 0.8 cm^{-1} , i.e. 24 GHz) was the first microwave spectrum to be observed, in fact, in the middle 1930s [18]. However, it took a further forty years of development of microwave spectroscopic methods before the observation of the inversion spectrum, corresponding to excited states, in the short-wave part of the submillimetre range (at 35 cm^{-1}) became possible.

3.1.2. Precise Digital Scanning of the BWO Output Frequency

The progress of methods of frequency stabilization of submillimetre BWOs, whose earlier state was detailed in references [19], [20] and [21], has now reached the stage where it is feasible to develop precise digital control of the output frequency and to have the possibility of digital frequency scanning [22, 23] analogous to that developed in the centimetre range [24, see also Chapter 1]. A block-diagram of a RAD spectrometer with precise digital control of the BWO frequency is given in Fig. 7.

The reference is provided by the signal from a frequency synthesizer operating in the conventional radiofrequency range [25]. The synthesizer frequency may be digitally scanned by the appropriate digital system. The stable synthesizer frequency (of the order of tens of MHz) is transferred up to the submillimetre frequency region (hundreds of gigahertz) by the use of a frequency multiplication chain consisting of a set of successive lock-in BWOs each appropriate to its increasing frequency range and connected together by frequency multipliers, formed from point-contact diodes. The submillimetre BWO frequency is thus rigidly linked to the synthesizer frequency and the problem of the measurement of the submillimetre frequency is automatically solved.

At the first stage of frequency multiplication, a radio-oscillator "flywheel" for the 200 MHz range is used which gives maximally stable and spectrally pure oscillations. The frequency of this oscillator is divided down, by parametric dividers, to the synthesizer range and the resulting frequency is mixed with that of the synthesizer to generate "beats". These are used to phase-lock the 200 MHz flywheel oscillator which has sufficient power to drive the subsequent multipliers, whose spectral output is pure enough (the spectrum of the synthesizer itself is unsatisfactory) and which now has the full stability of the synthesizer. When carrying out broad frequency scans,

† The results of a complete investigation of the ammonia spectrum near 1 THz, including precise measurements of the line frequencies, will be published elsewhere.

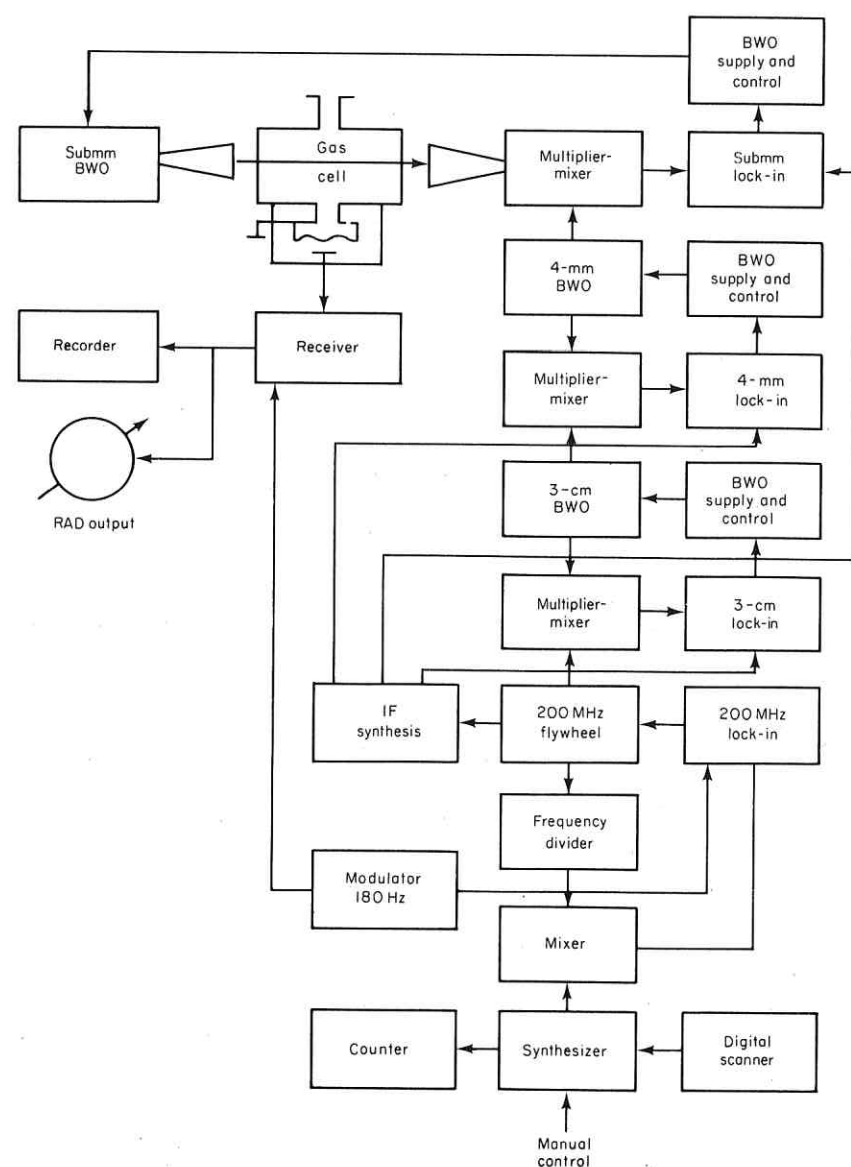


FIG. 7. RAD spectrometer with a system of precise digital scanning and measurements of more narrow regions of the spectrum in any part of the 150–600 GHz range. The accuracy of the frequency adjustment and the smallest step of digital scanning is $\sim 10^{-9}$. A recent version of this system, having one more AFC loop, has been successfully tested up to 1100 GHz.

an astatic servo-system is used in the lock-in loop of the radio-oscillator in addition to the electronic frequency control. This mechanically tunes the frequency of the resonant circuit following the synthesizer frequency. The frequency of the synthesizer is controlled by a synchronously operating counter.

At the subsequent stages of frequency multiplication, we have BWO lock-in systems for the 3 cm range, the 4 mm range and finally submillimetre BWOs for the 150–600 GHz range. A more detailed schematic of the last stages of the BWO lock-in system is shown in Fig. 8 of reference [9]. Due to

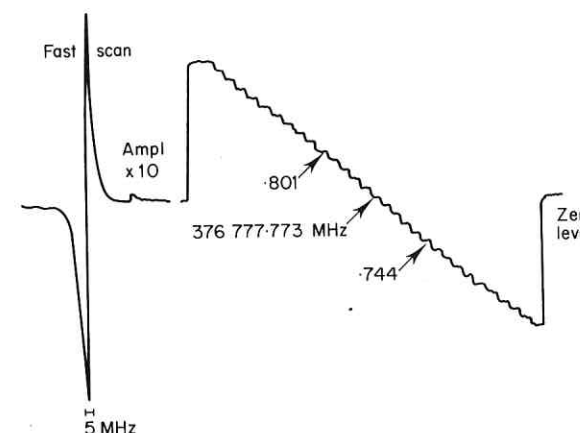


FIG. 8. The first record of a submillimetre N_2O spectral line obtained by RAD with the system of precise digital control of BWO frequency. On the left is the record of the line $J = 14 \rightarrow 15$ with fast digital scanning of the BWO frequency, on the right is the record of the central part of the same line with ten times increased amplification and slow digital scanning (in the opposite direction) of the BWO frequency. The scanning step 5672 Hz at the frequency ~ 377 GHz, is equivalent to a precision of 1.5×10^{-8} . The coefficient of the synthesizer frequency multiplication is 28360.

the fact that the synthesis of the lock-in system IF reference frequencies is derived from the same 200 MHz oscillation of the flywheel oscillator, the total coefficient of the frequency multiplication proves to be integral. The scanning of any desired submillimetre frequency region is now done by first manually tuning the radio oscillator to the appropriate frequency values, and setting the multiplication coefficients of the system. Then on the digital control unit, the values of the initial and final frequencies, the step and the rate of scanning and also the desired number of the scanning cycles are programmed. After this all the loops of the lock-in system are successively put into action and one can start the scanning regime. The selection of the corresponding multiplication coefficients as well as the putting into action

of the lock-in loops may be readily automated using the appropriate digital techniques [24]. Figure 8 shows the first record of a submillimetre spectral line obtained with digital program control of the BWO frequency in a RAD. To the left of this figure is shown a record of the $J = 14 \rightarrow 15$ line of N_2O near 377 GHz (12.57 cm^{-1}) obtained with fast digital scanning of the submillimetre BWO frequency. The line is recorded in the form of the first derivative of the absorption profile by introducing frequency modulation of the source by means of a sinusoidal voltage applied to the output of the detector of the first lock-in loop.[†] On the right is shown the central part of the same line recorded with the gain increased ten fold and with slow digital scanning of the submillimetre BWO frequency. The step of the frequency

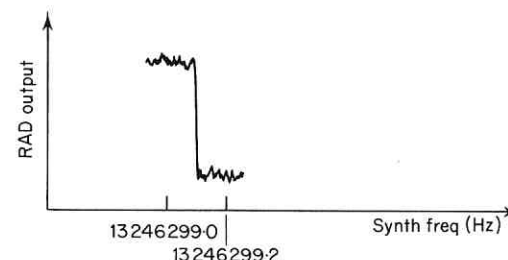


FIG. 9. Enlarged record of one "step" of N_2O line scanning $J = 14 \rightarrow 15$. Scanning step 0.2 Hz at the synthesizer frequency near 13 MHz, i.e. $\sim 1.5 \times 10^{-8}$. Coefficient of the synthesizer frequency multiplication 28444. The signal-to-noise ratio on the record is sufficient for the measurement of the frequency of the centre of the spectral line with an accuracy better than 10^{-9} .

scanning in this record is $\sim 1.5 \times 10^{-8}$ in relative units. On the left and on the right the level of zero output signal is recorded and the centre of the spectral line is taken to be that frequency where the signal crosses this zero level. Figure 9 shows one of the sample steps enlarged. It will be seen that the signal-to-noise ratio is good enough to permit the line-centre frequency to be defined to an accuracy of one part in 10^9 . This is at present the highest accuracy attainable in scanning submillimetre methods. However, caution is necessary because one will need to know all causes of systematic error before one can assume that the *defined* frequency is the *true* frequency of the line centre and so far a careful assessment of systematic error has not been carried out. Nevertheless the precision is now so high that, coupled with the ability of the RAD to work at reasonably large (up to tens of Torr), gas pressure it should be possible for the first time to undertake the precise study of submillimetre line-shifts produced by molecular collisions.

[†]The modulation must be symmetric to prevent an apparent shift of the line centre. Control to prevent asymmetry is made simply by taking measurements of the line-centre frequency at different values of the frequency deviation.

The actual bandwidth available in a scan varies from 3 GHz to 6 GHz up to 10–15 GHz depending on the exact location of the centre frequency in the submillimetre band. The scanning range is limited chiefly by imperfections in the construction of the last stage lock-in mixer-multiplier formed from a point-contact silicon diode. One may hope that with improvements of the mixer-multiplier broad-band characteristics, the region of continuous digital scanning without recourse to manual tuning can be considerably increased.

To summarize, the development of a system of precise digitally programmed control of BWO frequency in the 150–600 GHz region with an accuracy of 10^{-9} and radiation power ranging from units up to tens of milliwatts and of an analogous AFC system operating up to 1100 GHz, is a new and very important step in the progress of techniques for scanning coherent sources of radiation in the submillimetre frequency region and must lead to a re-estimation of the possibilities for spectroscopic investigations in this region.

3.2. The Cell and the Detector

The principal difference between a RAD cell and ones commonly used in submillimetre microwave spectrometers is the presence of a microphone inside the gas cell.[†] This creates specific problems in the optimal choice of the system "gas cell/acoustic detector" parameters as well as some particular construction problems. The solution of these problems will be considered in this section.

3.2.1. Calculation of Optimal RAD Cell and Detector Parameters

The pressure of the gas investigated in the RAD cell is determined by the resolution required for the experiment. The power of the radiation passing through the gas is limited either by the desired condition of spectral line saturation or else simply by the experimental conditions. To realize in this situation the maximal sensitivity of the RAD spectrometer, it is necessary to make the optimal choice of the gas cell/acoustic detector parameters to provide

- (1) The best possible transformation of the modulated radiation power absorbed into variations of gas pressure in the cell, and
- (2) Operation of the microphone down to the condition where it is limited only by the unavoidable thermal (Brownian) fluctuations of the gas pressure in the cell.

[†]As will be seen from Figs. 4 and 7, the microphone is conveniently placed not in the way of the radiation beam but in the side arm of the cell; however, strictly speaking, it is immersed in the gaseous medium of the cell and receives only the dynamic difference of pressure on the membrane due to the absorption of the modulated radiation in the absorption part of the cell.

To satisfy the first of these two conditions it is sufficient to fulfil the condition given in reference [9] equation (7) namely

$$\tau_{\text{mod}} \sim 2\pi\tau_{\text{cell}} \quad (3.2.1)$$

where τ_{mod} is the modulation period and τ_{cell} is the time of the thermal gas relaxation in the cell. This condition shows the desirability of altering the modulation frequency to match changes in the gas cell pressure.

The realization of the second condition was not so well covered in reference [9]. A more exact treatment has been given in [26] and will also be developed here. This will take into account all the sources of membrane fluctuations and also the dependence of the effective elasticity coefficient of the membrane on the voltage applied to the condenser microphone. It will also appear that the condition on the matching of the gas and membrane elasticities given in equation (8) of reference [9] is in fact unnecessarily strict.

To arrive at the condition where the acoustic detector (a condenser microphone in the gas plus an electronic high-frequency bridge microphone circuit) can register the thermal Brownian fluctuations of the gas in the cell, we consider on the one hand the sources of gas fluctuations in the receiving RAD system and their relative values, and on the other hand the sensitivity threshold of the electronic circuit due to fluctuations.

The effective elasticity coefficient of the membrane in the condenser microphone K_u , which depends on the voltage applied to the microphone, will enter into subsequent expressions. The electric field in the membrane-to-electrode gap is produced mainly by the high-frequency (ω_q) voltage of the bridge circuit supply V_q and to an extent by the constant voltage V_c necessary for the automatic tuning of the condenser microphone capacity (see Fig. 7 of reference [9]). The value of the static membrane elasticity in the presence of the voltage $V = V_q + V_c$ is defined as

$$K_u = K - \frac{CV^2}{d^2} = K \left(\frac{\alpha^2 - 1}{\alpha^2} \right), \quad (3.2.2)$$

where K is the self-elasticity coefficient of membrane itself, C is the capacity of the condenser microphone, d is the distance between the membrane and the other electrode and the averaging is carried out during a time much larger than the period of the electrical oscillations of the bridge supply but much less than the period of the mechanical membrane oscillations and the period of the modulation. The parameter α is defined to be $\alpha = d/d^*$ where $d^* = (CV^2/K)^{1/2}$ is the distance at which $K_u = 0$.

There are four aspects to be considered here.

(a) The fluctuations of the membrane (in vacuum) as a mechanical

oscillator of frequency Ω_M , quality factor of oscillation Q_M and elasticity coefficient K_u in the detector band $\Delta\omega_{\text{rec}}$ may be written as

$$\sigma_M \sim \left(\frac{2P_n}{\pi Q_M \Omega_M K} \right)^{1/2} \frac{\alpha}{(\alpha^2 - 1)^{1/2}}, \quad (3.2.3)$$

where

$$P_n \sim KT\Delta\omega_{\text{rec}}. \quad (3.2.4)$$

(b) The membrane fluctuations due to the gas surrounding it in the RAD cell at $m \ll 1$, written as

$$\sigma_m^g \sim \left(\frac{mP_n\tau_{\text{cell}}}{4\pi K} \right)^{1/2} \frac{\alpha}{(\alpha^2 - 1)^{1/2}}, \quad (3.2.5)$$

where m is the ratio of the gas and the membrane elasticities [9].

(c) The membrane fluctuations induced by electric fluctuations in the high-frequency resonant circuit of the condenser microphone. This source of fluctuations was not considered in [9]. Amplitude fluctuations of the high-frequency supply of the bridge, including the condenser microphone lead to fluctuational displacements of the membrane which are then transformed again into electrical phase† fluctuations. Calculation gives the following expression for fluctuations of this kind—under the assumption that the amplitude modulation is due to thermal resonant circuit noise only:

$$\sigma_m^i \sim \left(\frac{2P_n Q}{\omega_q K} \right)^{1/2} \frac{\alpha}{\alpha^2 - 1}, \quad (3.2.6)$$

where Q is the quality factor of the resonant circuit of the condenser microphone. These fluctuations are associated with the degree of influence of the electronic circuit on the membrane and, of course, go to zero as this influence is reduced to zero, i.e. as $\alpha \rightarrow \infty$.

(d) The fluctuational sensitivity threshold of the electronic circuit of the high-frequency bridge condenser microphone is

$$\sigma_e \sim 2 \left(\frac{P_n}{Q\omega_q K} \right)^{1/2} \alpha. \quad (3.2.7)$$

Thus the condition for obtaining the RAD limiting sensitivity will be

$$\sigma_m^g > \sigma_M + \sigma_m^i + \sigma_e. \quad (3.2.8)$$

This condition may be fulfilled by using the differences in the dependences of the intensity of the fluctuation sources on the parameters of the receiving

† If amplitude fluctuations are transformed also into amplitude fluctuations of the membrane (for example on the slope of the slightly detuned resonance circuit curve), then under certain conditions a mechanical instability (self-excitation of oscillations) of the membrane may occur. This is not the only source of mechanical instability of the membrane.

RAD system. In practice, the most important parameters are the frequency of the bridge supply ω_q and the degree of approach to the membrane instability condition defined by α . To analyse methods for fulfilling the condition (3.2.8) we note first that the terms σ_c and σ_m^i may (at least in principle) be made small enough in comparison with σ_m^g merely by increasing the bridge supply frequency ω_q . In order to prevent the induced noise σ_m^i from exceeding the inherent noise of the electronic circuit, conditions of the type $\alpha > Q^{1/2}$ must be satisfied, i.e. the membrane must be far from the instability. In practice this is not a convenient regime since it requires large voltages to be applied to the bridge and in general therefore the regime[†] $\sigma_m^i \sim \sigma_c$ is preferred. To fulfil now the condition $\sigma_m^g > \sigma_m^i$ (assuming of course that σ_c and σ_m^i are small enough), it is necessary to satisfy relations of the type

$$m\tau_{\text{cell}} Q_M F_M > 1, \quad (3.2.9)$$

where $F_M = \Omega_M/2\pi$. Estimates show that it is possible to fulfil this condition with realistic values of the parameters τ_{cell} , Q_M , F_M in the region $m \geq 10^{-2}$ which may also be achieved in practice. When the membrane is used at its mechanical resonance, the value m in the previous expressions must be replaced by mQ_M .

3.2.2. Construction and Operation of the Cell and the Detector of a RAD Spectrometer

The general construction of the RAD absorption cell equipped with microphone is clear from Figs. 4 and 7. The cell itself is a tube approximately 10 cm long and approximately 1.5 cm in diameter. The cell windows are made of teflon (polytetrafluorethylene) or else from crystal quartz plates. The microphone is placed in the side arm of the cell. Vibrational pick-up is a serious problem and to reduce it as much as possible the entire microphone assembly is connected to the main body of the cell by a single teflon tube which also serves as an acoustic channel to the absorbing part of the cell. The microphone membranes which are of the order of a few micrometres thickness are first glued to calibrated ring supports which are then mounted in the microphone assembly without further adjustment. The control of the distance between the membrane and the fixed electrode of the microphone is carried out by measurement of the microphone capacity and the control of the membrane elasticity coefficient by measurement of the variation of microphone capacity with applied

[†] It may be interesting to note that this consideration is a consequence of our unsuccessful attempts to increase the RAD sensitivity by using simply thinner and more flexible membranes, i.e. merely reducing K . The analysis given above shows that the problem is somewhat more complex.

voltage (the electrostatic attraction force acting on the membrane is easily calculated). The membranes can be made from teflon, from metallized mylar (polyethyleneterephthalate) and also from thin metal films, for example palladium film. The use of metallic membranes is convenient since it then becomes possible to heat the cell and thus employ vacuum cleaning. The microphone works well when the cell is cooled down to dry ice temperature. It also works well even when the cell is being continuously pumped so as to provide a "flow-through" regime. In one experiment, water vapour was pumped through the cell, from a bottle containing liquid water, by means of a vacuum pump and no significant increase in noise was noted.

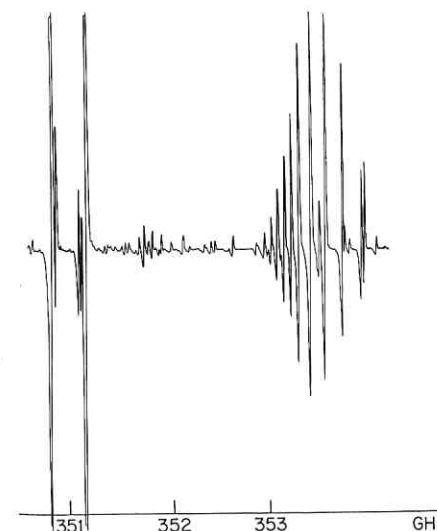


FIG. 10. A part of the submillimetre spectrum of a $\text{NO} + \text{NO}_2$ mixture recorded by RAD.

Of course, to reduce vibrational pick-up the vacuum pump was connected to the cell by means of a flexible pipe. Figure 10 gives a record of part of the spectrum of an $\text{NO} + \text{NO}_2$ mixture obtained with such a cell.

The block-diagram of the high-frequency bridge circuit of the condenser microphone presently used is given in Fig. 4. This circuit is considerably simplified compared to that given in reference [9] but there is no loss of sensitivity. The autotuning of the microphone capacity (i.e. balancing the bridge by means of the reactive component) is retained, but the bridge balance circuit using an active component is removed. The exact bridge balance, depending on the active component, does not change practically when using massive metallic membranes and even when one is using instead a metallized film, the resulting small disbalance of the bridge does not lead

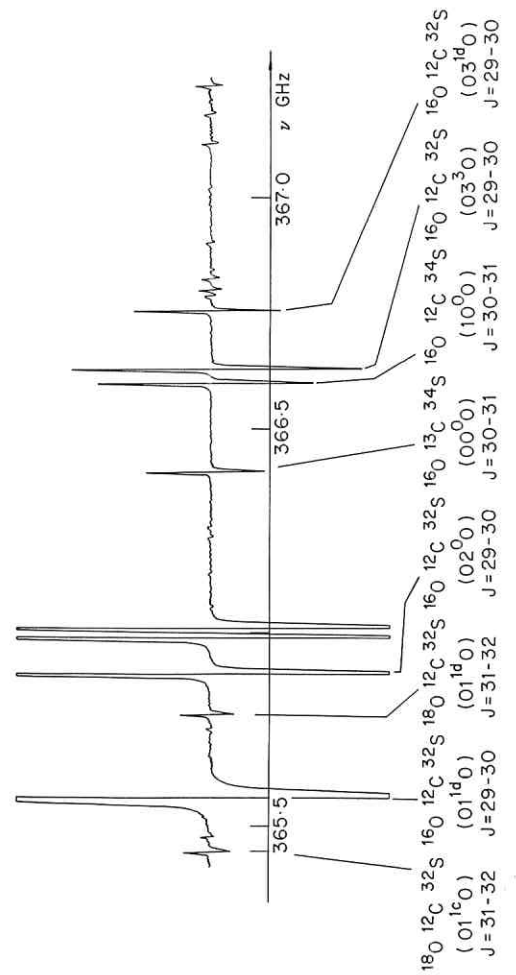


FIG. 11. A part of a submillimetre survey OCS spectrum used for measurements and assignments of the lines. On the record lines of $^{16}\text{O}^{13}\text{C}^3\text{S}$ in the natural abundance and vibrational satellites of the state (030) at room temperature are seen with rather good signal-to-noise ratio. The recording of the peak regions of the more intense lines is limited by the recorder.

to loss of sensitivity up to the point where the disbalance signal causes, because of overloading, an increase in the amplifier noise factor. The problem reduces therefore to the development of an amplifier having a sufficiently small noise factor at a finite signal value (i.e. relative to the small signal variations and not only to the small signal itself). Such an amplifier has been developed and this makes it possible to simplify both the adjustment and the operation of the circuit. The RAD sensitivity is illustrated by a recording of part of the OCS spectrum in the 366 GHz region shown in Fig. 11. Here will be seen lines due to vibrationally excited OCS at room temperature and also lines due to isotopic species. However, the signal-to-noise ratio is so good that it is possible to measure (with a frequency precision of one part in 10^8) the lines of $^{16}\text{O}^{12}\text{C}^{32}\text{S}$ in the vibrational state $v_2 = 4$ at room temperature and also the lines of $^{16}\text{O}^{13}\text{C}^{33}\text{S}$ at natural isotopic abundance!

4. PRACTICAL METHODS OF INVESTIGATION IN SUBMILLIMETRE MICROWAVE SCANNING SPECTROMETRY

The situation illustrated in Fig. 1 of a practically exact coincidence of the region covered by scanning submillimetre microwave spectrometry and the region of maximum intensity in the rotational spectrum of OCS ($B \sim 6$ GHz) is not unusual, since it is true for a broad class of light molecules and remains roughly true for many more molecules since the peak of intensity depends rather weakly on the rotational constant B ($v_{\max} \sim B^{1/2}$) [3]. In this situation it becomes possible to completely characterize the rotational spectrum of a desired molecule by a single measurement of its submillimetre absorption lines. Some examples of this are given later. With so many possibilities for meaningful experiments opened up in this way it is a problem to know where to begin and since the group at Gorky has no great experience in molecular spectroscopy, most of the investigations we have undertaken have tended to spring up spontaneously during the course of practical investigations. They can be regarded therefore as demonstrations of the power of the method but not as illustrations of its ultimate potential for yielding information on problems of contemporary interest.

Investigations begin with a survey record of the sample spectrum using the regime of broad-range fast scanning and including where necessary a reference spectrum. In the case of the OCS and N_2O spectra reported here, lines of known isotopic combinations and of known vibrationally excited states are used as references to identify the unknown ones. This survey

TABLE 3. Measured frequencies (v_m) and differences between measured and calculated frequencies ($v_m - v_c$) according to (4.1) of ground state rotational transitions ($J \rightarrow J+1$) of the OCS molecule.

record serves to define the regions to be covered more carefully later, to define the signal-to-noise values available with the various lines, to classify lines according to order of intensity for further help with the assignment and to list particular objects to be subsequently carefully examined using the precise scanning regime. When carrying out the subsequent measurements of the line frequencies with the stabilized BWO this broad survey acts like an overall map and the investigator constantly consults it to specify the object being measured. Line frequencies are marked on it and the process of further refinement of the positions and identities of the objects is also included on the survey. The agreement with the survey spectrum is the primary guarantee of the correct assignment of the lines. The survey record is also used for noting the cases of overlapping lines. These require either special processing (in an attempt to disentangle the contributing components) or else to be left out of the data reduction process. A part of such a survey record is given in Fig. 11. The complete record occupied tens of metres of the recorder chart and covered hundreds of gigahertz. The corresponding studies on N₂O have yielded continuous spectra stretching from 375–565 GHz [27].

The next step is the measurement of line frequencies under the regime where the BWO is stabilized against a reference signal. The measurement process (after establishing the BWO lock-in and defining the values of the frequency multiplication coefficients) consists of adjustment of the reference oscillator frequency to obtain zero output RAD signal. This is because the RAD operates in the source-modulation mode [see Chapter 1, section 2.3] and the spectral line therefore appears in first-derivative form. When the BWO tunes to give zero output, the frequency coincides exactly with the line-centre frequency. The frequency is then determined by noting the reference frequency value and multiplying by the appropriate scaling factor. Some examples of some experimental data obtained are given in Table 3. For N₂O, for example, frequencies have been measured for more than 160 lines of twenty-two spectroscopically different species (that is different vibrational states and different isotopic combinations of the molecule). For OCS, at present, frequencies have been measured of more than 500 lines belonging to approximately sixty spectroscopically different species of the molecule. Some examples of isotopic species are given in Table 3 and the complete reduction of all the data to give the rotational constants is given in Table 4. The precision with which these numbers have been determined can be gauged from the differences between calculated and observed line frequencies given also in Table 3. It will be seen that these differences are only of the order of a few kilohertz and this represents a precision of at least one part in 10⁸. The rotational constants themselves are obtained from a computer least-squares fit to the usual expression for the rotational energy,

TABLE 4. Effective rotational and centrifugal constants of the OCS molecule derived from a preliminary processing of our submillimetre experimental data

Vibrational state	B ^{eff} (MHz)	D ^{eff} (kHz)	H ^{eff} (10 ⁻³ Hz)
¹⁶ O ¹² C ³² S			
00 ⁰	6081.4950(37)	1.3053(54)	1.7(26)
01 ^{1c} 0	6088.9003(30)	1.3213(40)	0.2(17)
01 ^{1d} 0	6095.2610(28)	1.3247(36)	-0.1(15)
10 ⁰ 0	6063.3584(28)	1.3303(36)	0.4(15)
02 ^{2c} 0	6102.5714(28)	1.5716(36)	-2.3(15)
02 ^{2d} 0	6102.5686(28)	1.3400(36)	-2.1(15)
02 ⁰ 0	6100.1912(28)	1.0979(36)	2.2(15)
11 ^{1c} 0	6072.0801(31)	1.3535(40)	-1.1(17)
11 ^{1d} 0	6078.9237(32)	1.3553(42)	-4.8(19)
03 ^{3c,d} 0	6112.956(31)	1.4479(40)	-3.4(17)
03 ^{1d} 0	6114.8235(36)	1.2222(46)	-10.6(21)
20 ⁰ 0	6044.881(10)	1.366(14)	2.3(60)
12 ^{2c} 0	6087.176(16)	1.584(21)	-41.1(89)
12 ^{2d} 0	6087.219(10)	1.367(13)	-7.7(54)
12 ⁰ 0	6084.3516(93)	1.037(12)	-15.5(50)
00 ¹ 1	6045.123(18)	1.398(24)	31.6(96)
04 ^{4c,d} 0	6123.248(11)	1.465(14)	-2.8(58)
04 ^{2c} 0	6117.292(19)	1.924(24)	-24(10)
04 ^{2d} 0	6117.376(31)	1.321(39)	23(16)
04 ⁰ 0	6114.744(20)	0.517(25)	-29(10)
¹⁶ O ¹² C ³⁴ S			
00 ⁰ 0	5932.8326(40)	1.2400(48)	-0.7(19)
01 ^{1c} 0	5940.1290(28)	1.2582(35)	-0.7(14)
01 ^{1d} 0	5946.1990(28)	1.2635(35)	-0.2(14)
10 ⁰ 0	5915.1436(33)	1.2585(41)	-2.9(17)
02 ^{2c} 0	5953.4012(44)	1.5054(56)	-1.7(22)
02 ^{2d} 0	5953.3976(44)	1.2793(56)	-1.0(22)
02 ⁰ 0	5951.2603(45)	1.0455(56)	2.66(22)
11 ^{1c} 0	5923.6444(96)	1.292(12)	-0.1(46)
11 ^{1d} 0	5930.1385(96)	1.297(12)	-1.7(46)
03 ^{3c,d} 0	5963.535(25)	1.385(29)	-3(11)
¹⁶ O ¹³ C ³² S			
00 ⁰ 0	6061.9224(24)	1.2960(36)	-0.9(15)
01 ^{1c} 0	6068.6583(32)	1.3128(41)	-1.3(17)
01 ^{1d} 0	6075.1686(32)	1.3203(41)	0.0(17)
10 ⁰ 0	6043.9468(77)	1.3395(99)	3.9(40)

Continued over

Table 4—continued

Vibrational state	B^{eff} (MHz)	D^{eff} (kHz)	H^{eff} (10^{-3} Hz)
$^{16}\text{O}^{12}\text{C}^{33}\text{S}$			
00 ⁰ 0	6004.9168(39)	1.2713(50)	0.2(21)
01 ^{1c} 0	6012.2674(48)	1.2897(60)	-0.1(25)
01 ^{1d} 0	6018.4840(58)	1.3030(74)	4.2(31)
10 ⁰ 0	5987.0165(90)	1.305(11)	3.6(46)
02 ^{2c} 0	6025.732(14)	1.536(18)	-3.3(76)
02 ^{2d} 0	6025.733(14)	1.314(18)	0.4(76)
02 ⁰ 0	6023.475(15)	1.066(19)	0.2(82)
$^{18}\text{O}^{12}\text{C}^{32}\text{S}$			
00 ⁰ 0	5704.8504(42)	1.1256(46)	-2.6(17)
01 ^{1c} 0	5712.1613(73)	1.1470(85)	-1.0(34)
01 ^{1d} 0	5717.813(11)	1.148(12)	-2.1(48)
$^{16}\text{O}^{13}\text{C}^{34}\text{S}$			
00 ⁰ 0	5911.7180(35)	1.2197(44)	-7.2(18)
01 ^{1c} 0	5918.360(17)	1.239(20)	-6.2(77)
01 ^{1d} 0	5924.581(12)	1.261(15)	4.6(57)
$^{17}\text{O}^{12}\text{C}^{32}\text{S}$			
00 ⁰ 0	5883.6570(39)	1.1935(47)	-6.6(19)
01 ^{1c} 0	5891.008(32)	1.203(39)	-9(16)
01 ^{1d} 0	5897.026(33)	1.231(40)	-5(16)
$^{16}\text{O}^{12}\text{C}^{36}\text{S}$			
00 ⁰ 0	5799.6880(79)	1.1831(95)	-2.5(38)
$^{18}\text{O}^{12}\text{C}^{34}\text{S}$			
00 ⁰ 0	5559.973(11)	1.082(16)	1.2(38)
$^{16}\text{O}^{13}\text{C}^{33}\text{S}$			
00 ⁰ 0	5984.586(11)	1.294(14)	10.8(56)

viz:

$$E_R^{\text{eff}} = B^{\text{eff}}J(J+1) - D^{\text{eff}}J^2(J+1)^2 + H^{\text{eff}}J^3(J+1)^3. \quad (4.1)$$

The computer program is described in reference [9]. The results shown in Table 3 were obtained before the development of the system described in section 3.1.2. One may expect therefore to be able to improve the precision with which the rotational constants are known even further.

In order to be sure of the assignment, and this is especially important for the weak lines, all the experimental quantities are plotted on diagrams of the Loomis-Wood type [28, 9].

TABLE 5. $^{14}\text{N}_2^{16}\text{O}$ molecular constants

B_0		12 561.6368 (9)
α_1^*		58.6856 (630)
α_2^*	(MHz)	-17.037357 (520)
γ_{12}		-0.3641 (320)
γ_{22}		-0.1964 (160)
γ_{ll}		0.0251 (160)
D_0		5.28680 (240)
β_1	(kHz)	-0.04948 (190)
β_2		-0.083440 (460)
H_0	(Hz)	0.00619 (220)
$q_{(010)}$		11.87337 (120)
q_1	(MHz)	0.1757 (280)
q_2		0.05715 (690)
q_J		-19.46 (360)
q_{JJ}	(Hz)	0.00360 (330)
ρ		1.140 (300)
g_{ll}	(GHz)	14.377 (940)
Δ_1		2.9406
Δ_2		2.8976
$K_{(100)}^{122}$	(THz)	1.3425 (100)
λ_2		-0.01246 (290)
λ_J	(MHz)	-3.413 (100)

The mathematical processing referred to above is carried out by means of a set of computer programs. These are based on algorithms described in references [9], [29] and [30]. They include the "inverse" problem (i.e. from a set of line frequencies calculate a set of constants and the correlation matrix†) and thus calculate the constants B , D and H of a linear molecule, a set of rotational and rotational-vibrational interaction constants of a linear molecule (an example is given later), the commonly used constants Q_R , τ or the alternative constants Q and D of the asymmetric top introduced in reference [30]. It also includes the "direct" (i.e. set of constants plus correlation matrix gives frequencies and line intensities) problem for the same cases. The direct problem is a constituent part of the inverse one and it is used together with another programme for the correction of frequencies obtained from overlapping lines [27], etc. Examples of the results obtained are tabulated in Tables 4 and 5. The preliminary results for OCS given in Table 4 are obtained *only* from our measurements. A complete processing of

† The use of the correlation matrix technique is described in reference [9] and illustrated by several examples.

the OCS spectrum incorporating other microwave data will be published separately.

Table 5 gives similar results for the principal isotopic component of N₂O namely ¹⁴N¹⁴N¹⁶O. The results of the processing are more complete than the earlier values [27] since they also include data for the vibrational state (03³0). The definition of the constants corresponds to that given earlier [27]. The results listed in Tables 3–5 demonstrate the abundance of data on the rotational spectra of molecules which may be obtained, in a single investigation, by the methods of modern scanning submillimetre spectroscopy. The introduction of the system of precise digital frequency control in future experimental systems will lead to further simplification and should make possible at least a partial automation of the measurement process and also give an increase in sensitivity because the procedure of digital smoothing can be applied to the experimental results. Both these advances will increase the amount and the quality of the high-resolution submillimetre data.

5. CONCLUSION

It is now possible to make routine use on a widespread scale of the techniques of scanning submillimetre microwave spectrometry with sensitivity and accuracy not essentially different from the values found in the centimetre range. This is the beginning of the long-expected process of exploring the submillimetre region for the purpose of regular molecular spectroscopy. It seems that one can now say that the submillimetre region no longer *separates* but instead *connects* the neighbouring microwave and infrared regions. We can look forward to a steady stream of molecular data emerging from future studies using these powerful techniques of absorption spectroscopy in this very interesting region.

REFERENCES

- [1] Gordy, W. (1960). In "Proc. Symp. Millimeter Waves", Polytechnic Press of the Polytechnic Institute of Brooklyn, New York; (1965) *Pure Appl. Chem.* **11**, 403.
- [2] Townes, C. H., Schawlow, A. L. (1955). "Microwave Spectroscopy". McGraw-Hill, New York.
- [3] Gordy, W., Cook, R. L. (1970). "Microwave Molecular Spectra". Wiley Interscience, New York.
- [4] Martin, D. (ed.) (1967). "Spectroscopic Techniques, Far Infrared, Submillimeter and Millimeter Waves". North-Holland, Amsterdam.

4. MODERN SUB MM MW SCANNING SPECTROMETRY

- [5] Chantry, G. W. (1971). "Submillimeter Spectroscopy". Academic Press, London, New York.
- [6] Golant, M. B., Vilenkin, R. L., Zyulina, E. A., Kaplun, Z. F., Negirev, A. A., Parilov, V. A., Rebrova, T. F., Savel'ev, V. S. (1965). *PTE* **N4**, 136; Golant, M. B., Alekseenko, Z. T., Korotkova, Z. S., Lukina, L. A., Negirev, A. A., Petrova, O. P., Rebrova, T. F., Savel'ev, V. S. (1969). *PTE* **N3**, 231.
- [7] Krupnov, A. F., Gershtein, L. I., Shustrov, V. G., Belov, S. P. (1970). *Izv. VUZ. Radiofizika* **13**, 1403; Belov, S. P., Burenin, A. V., Gershtein, L. I., Kasakov, V. P., Karyakin, E. N., Krupnov, A. F. (1973). *JETP Lett.* **18**, 285; Belov, S. P., Burenin, A. V., Gershtein, L. I., Korolikhin, V. V., Krupnov, A. F. (1973). *Opt. Spektrosk.* **35**, 295; Burenin, A. V., Krupnov, A. F. (1974). *Izv. VUZ. Radiofizika* **17**, 1242; Antakov, I. I., Belov, S. P., Gershtein, L. I., Ginzburg, V. A., Krupnov, A. F., Parshin, G. S. (1974). *JETP Lett.* **19**, 634.
- [8] Bell, A. G. (1881). *Phil. Mag.* **11**, 510; Röntgen, W. C. (1881). *Phil. Mag.* **11**, 308; Tyndall, J. (1881). *Proc. Roy. Soc. London* **31**, 307.
- [9] Krupnov, A. F., Burenin, A. V. (1976). In "Molecular Spectroscopy: Modern Research" (K. N. Rao, ed.) Vol. II, pp. 93–126. Academic Press, New York.
- [10] Krupnov, A. F. (1975). *JETP* **69**, 1981.
- [11] Lamb, W. E., Jr. (1964). *Phys. Rev.* **134A**, 1429.
- [12] Shimoda, K. (1973). *Appl. Phys.* **1**, 77.
- [13] Harrington, H. W. (1967). *J. Chem. Phys.* **46**, 3698; (1970). **49**, 141.
- [14] Vinogradov, E. A., Irisova, N. A., Mandel'shtam, T. S., Shimaonov, T. A. (1967). *PTE* **N5**, 192; Zvereva, G. A., Irisova, N. A., Mandel'shtam, T. S., Prokhorov, A. M. (1970). *DAN* **193**, 791.
- [15] Dryagin, Yu. A. (1970). *Izv. VUZ. Radiofizika* **13**, 141.
- [16] Gershtein, L. I. (1976). *III All-Union Symposium on Molecular Spectroscopy at High and Super-high Resolution, Novosibirsk* (1976). Abstracts, p. 70.
- [17] Belov, S. P., Burenin, A. V., Gershtein, L. I., Karyakin, E. N., Korolikhin, V. V., Krupnov, A. F. (1973). *PTE* **N6**, 206.
- [18] Cleeton, C. E., Williams, N. H. (1934). *Phys. Rev.* **45**, 234.
- [19] Krupnov, A. F., Gershtein, L. I. (1970). *PTE* **N1**, 159.
- [20] Krupnov, A. F., Gershtein, L. I. (1970). *PTE* **N6**, 143.
- [21] Val'dov, A. N., Gershtein, L. I., Karyakin, E. N., Krupnov, A. F., Maslovsky, A. V. (1974). *PTE* **N5**, 110.
- [22] Krupnov, A. F., Burenin, A. V. (1976). 4th Int. Seminar on High Resolution IR Spectroscopy, paper DI, Prague.
- [23] Gershtein, L. I., Maslovsky, A. V., Belov, S. P. (1976). *III All-Union Symposium on Molecular Spectroscopy at High and Super-High Resolution, Novosibirsk* (1976). Abstracts, p. 65.
- [24] Harrington, H. W., Hearn, I. R., Rauskolb, R. F. (1971). *Hewlett-Packard J.* **22**, 2.
- [25] Blagov, V. A., Dombrovsky, A. S., Zaitsev, V. N., Panteleev, A. V., Ul'yanov, A. A., Fateev, B. P. (1971). "Apparatus for Frequency and Time Measurements" (A. P. Gorshkov, ed.) Sovet Radio M.
- [26] Gershtein, L. I., Shurin, Yu. M. (1976). *III All-Union Symposium on Molecular Spectroscopy at High and Super-High Resolution, Novosibirsk* (1976). Abstracts, p. 66.
- [27] Andreev, B. A., Burenin, A. V., Karyakin, E. N., Krupnov, A. F., Shapin, S. M. (1976). *J. Mol. Spectrosc.* **62**, 125.

- [28] Scott, I. F., Rao, K. N. (1966). *J. Mol. Spectrosc.* **20**, 461; Ghergesi, S., Rao, K. N. (1968). *J. Mol. Spectrosc.* **28**, 27; Mantz, A. W., Rao, K. N. (1969). *J. Mol. Spectrosc.* **30**, 513.
- [29] Andreev, B. A., Burenin, A. V., Krupnov, A. F., Shchapin, S. M. (1975). *Opt. Spektrosk.* **39**, 864.
- [30] Burenin, A. V., Krupnov, A. F., Yagnetinsky, A. B. (1974). *Izv. VUZ Radiofizika* **17**, 1136.
- [31] Smith, S. D. (1976). In "Very High Resolution Spectroscopy" (R. A. Smith, ed.), p. 13, Academic Press, London; (1975). 4th Colloquium on High Resolution Molecular Spectroscopy" paper F.I, Tours.

APPENDIX 1

Calculation of Sub-Doppler Spectral Line-shapes

The calculation of the shape of sub-Doppler spectral lines is appropriate to the cell configuration shown in Fig. 12. We limit the problem to the two-dimensional case, i.e. the configuration does not depend on the z coordinate. In the absence of the partitions limiting the molecular motion the shape of the spectral line observed in RSCS, at sufficiently low pressures of the gas, is defined by the Doppler effect due to the thermal motion of molecules. If we take into account that a molecule with a velocity u_x interacts with the radiation propagating along the axis x at the frequency $\omega_s = \omega_0(1+u_x/c)$ and the number of molecules having velocities in the interval $u_x, u_x + du_x$ is defined by the one-dimensional Maxwell distribution as

$$n(u_x) du_x = \frac{1}{u_t \sqrt{\pi}} \exp(-u_x^2/u_t^2) du_x, \quad (\text{A1.1})$$

(where $u_t = (2kT/M)^{1/2}$ is the most probable velocity of molecules in the gas), then at a sufficiently small homogeneous line-width, the expression (A1.1) with the substitution

$$u_x = c \frac{\omega_s - \omega_0}{\omega_0} \quad (\text{A1.2})$$

gives the Doppler line form. The presence of partitions changes the u_x distribution of those molecules which are excited by the radiation field in region I (see Figs. 2 and 12) and which then enter region II without collisions with partitions, in comparison with the distribution of the form (A1.1). It is just these molecules that take part in the formation of the signal from the spectral line. Then to calculate the shape of the line observed, it is sufficient to obtain the expression for this changed distribution of molecules absorbing quanta of radiation in region I and entering without collision region II and then substitute u_x from equation (A1.2).

The free-flight condition (see Fig. 12, where one of the channels formed by the partitions is shown) for a molecule entering a channel at the point x' with velocities u_x, u_y will be

$$u_y > \frac{L}{a - x'} u_x, \quad (\text{A1.3})$$

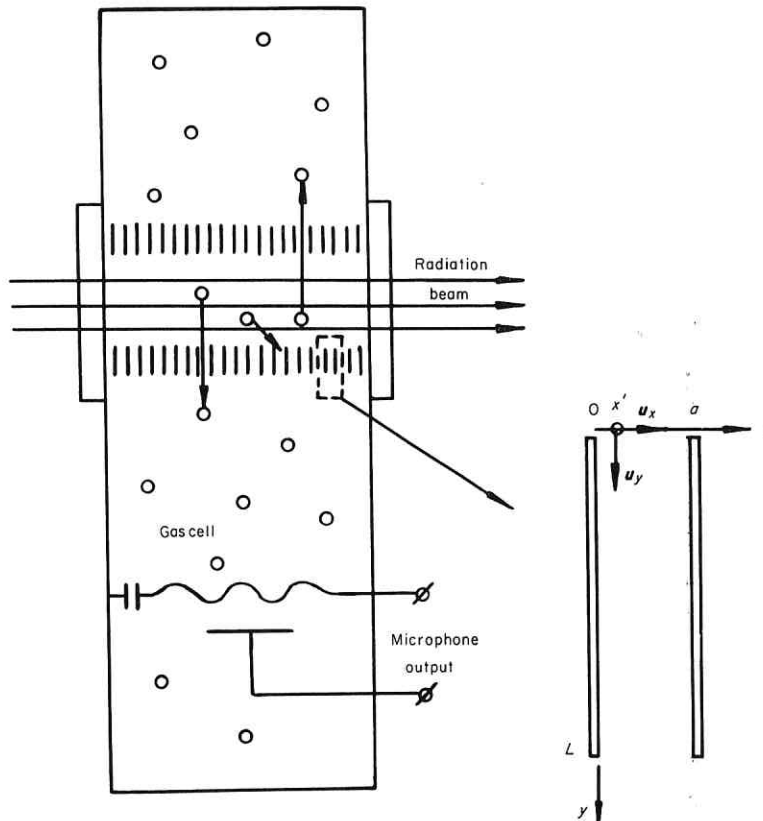


FIG. 12. A possible configuration of a RAD cell to obtain sub-Doppler lines. To heat the gas in the cell (i.e. to produce the acoustic signal from the line) excited molecules are only used which are free from the Doppler shift. The conditions for obtaining sub-Doppler lines are given in section 2. To form the acoustic signal (i.e. to thermalize the gas in the cell) the characteristic dimensions of the gas cell must be larger than the mean-free-path of the molecules. On the right a detail section of the diaphragms (partitions) is shown performing the velocity selection (one channel). The thermal time constant of diaphragms must be much larger than the thermal time constant of the gas in the cell.

where the symbols are clear from the figure. Then the fraction of molecules from (A1.1) passing the channel without collisions will be equal to

$$\delta(u_x) = \frac{2}{u_t^2} \int_{Lu_x/(a-x')}^{\infty} u_y \exp(-u_y^2/u_t^2) du_y \\ = \exp\left[-\left(\frac{L}{a} \frac{u_x}{u_t}\right)^2 \frac{1}{(1-s)^2}\right], \quad (\text{A1.4})$$

where $s = x'/a$ and, averaging over entrance points x' in the interval $0-a$, we

obtain for the u_x distribution of molecules transporting the excitation from region I to region II,

$$n'(u_x) du_x = \frac{1}{u_t \sqrt{\pi}} \exp(-u_x^2/u_t^2) \int_0^1 \exp\left[-\left(\frac{L}{a} \frac{u_x}{u_t}\right)^2 \frac{1}{(1-s)^2}\right] ds. \quad (\text{A1.5})$$

The integral in equation (A1.5) is not expressible in terms of elementary functions; however, it is easy to see that (A1.5) defines a velocity distribution $n'(u_x)$, which may be essentially narrower than the initial one (A1.1). The first factor in the exponent under the integral has the form $(Lu_x/a)^2/u_t^2$ instead of u_x^2/u_t^2 in (A1.1); and, in addition, the distortion of the velocity distribution due to the dependence of the free-flight condition (A1.3) on the entrance point leads to a further line-narrowing. Naturally the maximum amplitude of the signal from the line (the signal at the centre of the line) does not change, since partitions do not interfere with molecules with $u_x = 0$. The line-shape at the given value of $\theta = a/L$ is easily found from (A1.5) numerically. At $\theta \ll 1$ the first exponent in (A1.5) may be assumed to be equal to unity. Figure 3 gives the line-shape corresponding to a molecular u_x distribution of the form (A1.5) and $\theta = 0.1$. The abscissa axis scale is expressed in units of the initial Doppler line half-width, in the gas, between the half-intensity points,

$$\Delta\omega_D \simeq 0.84(u_t/c)\omega_0. \quad (\text{A1.6})$$

From Fig. 3 it is seen that such cutting of the velocity distribution leads to a rather sharp form for the central peak of the line (the discontinuity of the line-shape derivative at the line centre is a consequence of the assumption of a negligibly small homogeneous line-width; in practice, the central peak will be "rounded" by the homogeneous broadening which is defined, for example, by the time of flight of molecules through the region of the radiation field). The half-width between half-intensity points of the line obtained at $\theta = 0.1$ is

$$\Delta\omega \simeq 0.04\Delta\omega_D. \quad (\text{A1.7})$$

It is important to note that deviations from perpendicularity of partitions and the direction of the radiation propagation in the axially symmetric cell design will not evidently lead to a shift of the observed line centre since for the every molecule moving in one direction there is in the gas a symmetrical one moving in just the opposite direction. Then the deviation from perpendicularity causes only a symmetric broadening of the line observed (which in the limit, with the partitions parallel to the direction of the radiation propagation, transforms to the usual Doppler line).

APPENDIX 2

Calculation of the Line-shape and Magnitude of the Signal from Lines in RSC Spectrometry under the Condition of Line Saturation

Let us consider the magnitude and the line-shape of a signal, from a spectral line in RSCS, associated with the electric dipole interaction of a linearly polarized (along the z axis) electromagnetic field with the pure rotational motion of a molecule. The line is assumed to be uniformly broadened, the optical depth to be small, and it is further assumed that there is a uniform intensity distribution of the radiation field over the absorption cell cross section.[†] For these typical conditions we have

$$A = GP_s(v, P_0),$$

$$P_s(v, P_0) = \pi \frac{(hv)^2}{kT} \Delta\nu_1 N f S l \sum_M \frac{\chi_M \Delta\nu_2}{(v - v_0)^2 + \Delta\nu_2(1 + \chi_M)}. \quad (\text{A2.1})$$

Here A is the magnitude of the signal, G is the constant characterizing the apparatus, v, P_0 are the frequency and the power of the electromagnetic radiation passing through the cell with a cross section S and a length l ; P_s is the power absorbed at the frequency by the spectral line consisting of a set of electric dipole rotational transitions $\Sigma_M(|J_1\tau_1M\rangle \rightarrow |J_2\tau_2M\rangle)$, where M is the magnetic quantum number defining the orientation of a molecule in space relative to the field and the summation is carried out in the limits $|M| \leq J = \min(J_1, J_2)$; v_0 is the central frequency of the spectral line; $\Delta\nu_1 = 1/2\pi T_1$; $\Delta\nu_2 = 1/2\pi T_2$ are associated with the time of the longitudinal (T_1) and the transverse (T_2) relaxation (for the rotational molecular spectrum in the gas phase T_1 usually equals T_2 [2]); N is the number of molecules per unit of volume; f is the portion of molecules in the energetic state $|J_1\tau_1M\rangle$, $\chi_M = P_0/P_M$, where

$$P_M = \frac{3}{8\pi} \cdot \frac{ch^2 \Delta\nu_1 \Delta\nu_2}{|\mu_{12}|_M^2(g)} \quad (\text{A2.2})$$

[†]For a submillimetre RAD spectrometer the operational range of the wavelength is $\sim 1.5\text{--}0.3$ mm, the cell length is ~ 10 cm, and the transverse section is near 1 cm^2 ; this permits one to have the cell entirely in the geometrical optics region, i.e. to obtain a uniform cell illumination by the radiation.

characterizes the power necessary for the saturation of the transition $|J_1\tau_1M\rangle \rightarrow |J_2\tau_2M\rangle$; g is the index of the principal rotational axis of a molecule.

Further it is convenient to introduce the following quantities

$$\chi = \frac{\sum_M \chi_M}{\sum_M 1} = \frac{8\pi}{3} \frac{\mu_g^2}{ch^2 \Delta\nu_1 \Delta\nu_2} \frac{P_0}{S} \frac{S_{J_1\tau_1 J_2\tau_2}(g)}{\sum_M 1} \quad (\text{A2.3})$$

$$z = (v - v_0)/\Delta\nu_2 \quad (\text{A2.4})$$

$$P_s^{\max} \simeq P_s(z = 0, x \rightarrow \infty) = \pi \frac{(hv_0)^2}{kT} \Delta\nu_1 N f S l \sum_M 1, \quad (\text{A2.5})$$

where μ_g is the component of the molecule dipole moment along the principal g axis,

$$S_{J_1\tau_1 J_2\tau_2}(g) = \frac{1}{\mu_g^2} \sum_M |\mu_{12}|_M^2(g)$$

is the spectral line strength. As a result,

$$P_s \simeq P_s^{\max} \phi(z, x), \quad (\text{A2.6})$$

$$\phi(z, x) = \left(\sum_M 1 \right)^{-1} \sum_M \frac{\chi_M}{z^2 + 1 + \chi_M}, \quad (\text{A2.7})$$

$$\chi_M = 3\chi \frac{J_1^2 - M^2}{J_1(2J_1 + 1)}; \quad P\text{-branch}, \quad -J_1 + 1 \leq M \leq J_2 - 1,$$

$$\chi_M = 3\chi \frac{M^2}{J_2(2J_2 + 1)}; \quad Q\text{-branch}, \quad -J_2 \leq M \leq J_2, \quad (\text{A2.8})$$

$$\chi_M = 3\chi \frac{J_2^2 - M^2}{J_2(2J_2 + 1)}; \quad R\text{-branch}, \quad -J_2 + 1 \leq M \leq J_2 - 1.$$

The shapes of the function $\phi(z, x)$ for P - and R -branches coincide after substitution $J_1 \leftrightarrow J_2$. Thus, it is sufficient to consider spectral lines only of the Q - and R -types. As $\chi \rightarrow 0$, $\phi \rightarrow 1/(z^2 + 1)$, i.e. the usual Lorentz absorption line is obtained.

For transitions between rotational terms with large values of the total angular momentum quantum number J (i.e. those typical for the case of submillimetre absorption lines) it is convenient to use the following approximate expression instead of (A2.7):

$$\phi^*(z, x) = \lim_{J \rightarrow \infty} \phi(z, x) = \begin{cases} 1 - \delta \operatorname{artg}(1/\delta) & (Q\text{-branch}) \\ 1 - (\delta' - 1/\delta') \operatorname{arth}(1/\delta') & (R\text{-branch}) \end{cases} \quad (\text{A2.9})$$

Here $\delta = [(z^2 + 1)/3\chi]^{1/2}$, $\delta' = (2\delta^2 + 1)^{1/2}$. The numerical calculation in the limits $10^{-2} \leq \chi \leq 10$, $0 \leq z \leq 10$, $1 \leq J \leq 25$ shows that the maximum difference between the exact (A2.7) and the approximate (A2.9) expressions observed at small values of J does not exceed a few per cent. As $\chi \rightarrow 0$, $\phi^* \rightarrow \chi/(z^2 + 1)$, i.e. it smoothly transforms to the exact expression.